The Astronomical Journal, 166:185 (10pp), 2023 November https://doi.org/10.3847/1538-3881/acf4f4

Systematically Measuring Ultradiffuse Galaxies (SMUDGes). IV. Ultradiffuse Satellites of Milky Way Analogs

Hina Goto[1], Dennis Zaritsky[1], Ananthan Karunakaran[2], Richard Donnerstein[1], and David J. Sand[1]
[1] Steward Observatory and Department of Astronomy, University of Arizona, 933 N. Cherry Ave., Tucson, AZ 85721, USA
[2] Instituto de Astrofísica de Andalucía (CSIC), Glorieta de la Astronomía, E-18008 Granada, Spain
Received 2023 February 6; revised 2023 August 25; accepted 2023 August 28; published 2023 October 5

Abstract

To better understand the formation of large, low-surface-brightness galaxies, we measure the correlation function between ultradiffuse galaxy (UDG) candidates and Milky Way analogs (MWAs). We find that: (1) the projected radial distribution of UDG satellites (projected surface density $\propto r^{-0.84\pm0.06}$) is consistent with that of normal satellite galaxies; (2) the number of UDG satellites per MWA ($S_{\rm UDG}$) is $\sim 0.5 \pm 0.1$ over projected radii from 20 to 250 kpc and $-17 < M_r < -13.5$; (3) $S_{\rm UDG}$ is consistent with a linear extrapolation of the relationship between the number of UDGs per halo versus halo mass obtained over galaxy group and cluster scales; (4) red UDG satellites dominate the population of UDG satellites ($\sim$80%); (5) over the range of satellite magnitudes studied, UDG satellites comprise $\sim$10% of the satellite galaxy population of MWAs; and (6) a significant fraction of these ($\sim$13%) have estimated total masses $>10^{10.9}\ M_\odot$ or, equivalently, at least half the halo mass of the LMC, and populate a large fraction ($\sim$18%) of the expected subhalos down to these masses. All of these results suggest a close association between the overall low-mass galaxy population and UDGs, which we interpret as favoring models where UDG formation principally occurs within the general context of low-mass galaxy formation over models invoking more exotic physical processes specifically invoked to form UDGs.

Unified Astronomy Thesaurus concepts: Low surface brightness galaxies (940); Galaxy properties (615)

1. Introduction

The success of the Λ CDM paradigm as a predictive framework for structure formation is nearly complete, with the only unresolved issues remaining at small galaxy ($\ll L^*$) scales (for an overview see Weinberg et al. 2015). The study of low-mass galaxies is then expected to highlight important baryonic physical evolutionary processes that may be missing in the simulations and, perhaps even more excitingly, potential departures from the canonical CDM phenomenology. The desire for progress on either of these two fronts has motivated significant efforts to improve the empirical study of low-mass galaxy populations (such as the deep galaxy searches undertaken within a variety of nearby environments; Crnojević et al. 2016; Park et al. 2017; Venhola et al. 2017; Ferrarese et al. 2020; La Marca et al. 2022b).

A particular class of low-mass galaxy is that of the satellite galaxy. Satellites lie within an even larger halo of a parent or host system. We focus here on satellite galaxies lying within the halos of $\sim L^*$ galaxies that we refer to as Milky Way analogs (MWAs). Due to gravitational and hydrodynamical interactions with these parent galaxies, simulations suggest that the numbers, internal structure, and star-formation histories of such satellites may have been altered relative to what they would have been for the same galaxies in isolation (for recent examples of such work see Martin et al. 2021; Samuel et al. 2022). As such, there are a variety of reasons to compare samples of satellite galaxies to samples of similar mass galaxies that do not consist exclusively of satellites (e.g., that of Blanton et al. 2005).

Broadly, there are two approaches used to search for satellite galaxies. In the first, which we refer to as "photometric," imaging is used to identify potential satellites around a set of selected parent galaxies. Typically, the redshifts are known for the parent galaxies but not for the candidate satellites. One measures the bulk satellite properties by evaluating the excess population of candidates projected in the vicinity of the parent galaxies (Holmberg 1969; Lorrimer et al. 1994; Sales & Lambas 2005; Guo et al. 2012; Wang & White 2012; Sales et al. 2013; Greene et al. 2022). Because foreground and background objects generally greatly outnumber satellites, large samples are needed to tease out results. In this approach one is able, for example, to reach conclusions regarding the radial density profile of satellites around parents, but not to determine which of the many candidates are true satellites. With the advent of large area photometric surveys, this approach now brings statistical power to the questions at hand and subsamples can be defined to explore properties of the satellite galaxy population. In the second approach, which we refer to as "spectroscopic," one measures redshifts of the satellite candidates and identifies those sharing the parent's redshift to within allowances for different peculiar velocities (Zaritsky et al. 1993; Prada et al. 2003; Geha et al. 2017). This approach does then allow for follow up of the true satellites and for an examination of the satellite kinematics but comes at great observational expense because it requires spectroscopy of many faint targets, most of which are contaminants. As such, it currently provides lower precision on the determination of certain bulk properties of satellites, such as the radial density profile, and is, of course, limited to satellites that are within spectroscopic reach. For low-surface-brightness galaxies, a spectroscopic approach is not feasible given that exposure times of $\sim$1 hr are needed on large telescopes to obtain a redshift (e.g., van Dokkum et al. 2015b; Chilingarian et al. 2019; Kadowaki et al. 2021).

Both of these approaches are limited by the initial selection of the candidate satellites, which is based on imaging and will always suffer from a surface brightness selection effect (spectroscopic surveys suffer an additional surface brightness bias because of the further difficulty in obtaining the spectra and a color bias because it is easier to measure redshifts for star-forming galaxies). The recent appreciation that there are many fairly large galaxies—large both in physical size (effective radius, r_e, $\geqslant$1.5 kpc) and total luminosity (some as bright as $M_g \sim -17$)—that have evaded detection due to their exceedingly low central surface brightness, and that such galaxies survive in dense environments (van Dokkum et al. 2015a), leads to a suspicion that previous satellite samples may be missing satellites that are as massive as the Large Magellanic Cloud (e.g., DF 44 has $M_{200} = 10^{11.2\pm0.6}\ M_\odot$; van Dokkum et al. 2019).

This suspicion prompted the recent examination of the deepest available samples of satellite galaxies outside the Local Group (Carlsten et al. 2021; Mao et al. 2021; Nashimoto et al. 2022) by Karunakaran & Zaritsky (2023) for what those samples imply regarding the existence of low-surface-brightness, physically-large galaxies (commonly referred to as ultradiffuse galaxies; UDGs[3]) as satellites of MWAs. Their conclusion was that MWAs host proportionally, by total mass, nearly the same number of UDGs as do more massive halos.

On its surface, this result suggests that UDG formation is neither enhanced nor inhibited in the galactic environment relative to outside that environment. Nevertheless, the sample of UDG satellites in that study consisted of only 41 confirmed[4] satellites split among 75 parent galaxies, making it difficult to divide the sample into categories and address additional questions. Encouragingly, consistent conclusions regarding the mean number of such satellites for MWAs were presented by Li et al. (2023b), who use an enhanced photometric approach that incorporates size and color to help remove contamination from a sample without spectroscopic follow up.

We return to the photometric approach with a large sample of UDG candidates and focus on bulk UDG satellite properties. We undertake this study because there now exists a catalog of UDG candidates that spans nearly 20,000 sq. degrees of sky and contains nearly 7000 candidates (the SMUDGes catalog; Zaritsky et al. 2019, 2022, 2023). We aim to establish the radial number density profile, the luminosity function, and the color distribution of UDG satellites of MWAs and compare those to the corresponding measurements of the more classical satellite population. By doing so, we will present conclusions regarding plausible UDG formation and evolution models. We present the technical aspects of the approach in Section 2 and our results and interpretation in Section 3. We use a standard WMAP9 cosmology (Hinshaw et al. 2013), although the results are insensitive to different choices of cosmological parameters at the level of current uncertainties, and magnitudes are from SDSS/DESI and are thus on the AB system (Oke 1964; Oke & Gunn 1983).

[3] These galaxies are, by convention, defined using a size criterion: most often but not exclusively that r_e is $\geqslant$1.5 kpc, and a surface brightness criterion, most often but not exclusively that the central surface brightness in the $g-$band is $\geqslant$24 mag arcsec^{-2}.

[4] 17 confirmed with spectroscopic redshifts and 24 with distances measured using surface brightness fluctuations.

2. Methodology

We use the SIMBAD database (Wenger et al. 2000) to identify MWAs projected in proximity to each UDG candidate in our catalog that meets a minimum 20% estimated completeness. For details of the completeness calculation see Zaritsky et al. (2022), though this criterion corresponds to an estimate that we have found >20% of the UDG candidates with similar photometric properties across the full survey footprint. We impose this cut to avoid having to make large, highly uncertain completeness corrections. Overall the completeness is roughly 50% in SMUDGes, due mainly to aggressive masking of the survey area around bright foreground objects and regions of Galactic Cirrus. An important related concern is that the completeness is expected to fall dramatically near each MWA because those regions were masked in the original UDG search (Zaritsky et al. 2022). That incompleteness factor is included in an average sense in the catalog because we account for the masked area; however, it is not mapped specifically around each MWA. As such, the distribution of pair separations will be increasingly incorrect at ever smaller separations; but, for the most part, we work at projected radii where we do not expect this to have an impact. Nevertheless, we search for signs of this effect in the results discussed below.

Using the absolute magnitude of the Milky Way ($M_g = -21.0$; Bland-Hawthorn & Gerhard 2016), we define MWAs to have $-22 < M_g < -20$ in three different recessional velocity slices ($4500 < cz/(\mathrm{km\ s^{-1}}) < 5500$, $5500 < cz/(\mathrm{km\ s^{-1}}) < 6500$, and $6500 < cz/(\mathrm{km\ s^{-1}}) < 7500$), which correspond in total to a redshift range of 0.015–0.025. The three slices provide us with independent checks of the results although we are only close to complete to the lower limit in UDG size ($r_e = 1.5$ kpc) in the nearest slice. Caution is also warranted when comparing among results from different studies, as the definition of MWA varies among studies focusing on such objects (e.g., Mao et al. 2021; Carlsten et al. 2021), which often have additional environmental conditions or, perhaps less critically, slightly different magnitude criteria. We impose the lower cz limits on the parents to ensure that candidate UDGs, which are selected in SMUDGes to have $r_e > 5\farcs3$, match the physical size criterion of UDGs ($r_e \geqslant$ 1.5 kpc; van Dokkum et al. 2015a). We limit the redshift range of each slice to minimize possible variations in satellite magnitude and size within each sample. We adopt an upper size limit ($r_e < 6$ kpc), which is not a standard UDG criterion, because UDG candidates with inferred sizes larger than this limit are likely contaminants (Kadowaki et al. 2021; Zaritsky et al. 2022; Karunakaran & Zaritsky 2023). To include potential MWAs without a cataloged value of m_g that do have a cataloged value of m_B, we calculate the average $m_g - m_B$ color for those with photometry in both bands and apply that value as a correction to m_B for those missing m_g. This is a crude correction but we only use the parent magnitude to place it relative to the two magnitude wide bin defining MWAs.

We set the search radius for MWAs around each UDG candidate in the completed SMUDGes catalog (Zaritsky et al. 2023) to correspond to 10 Mpc at the near edge of each recessional velocity slice because that separation corresponds roughly to where the galaxy–galaxy correlation function drops below a value of 1 (Tucker et al. 1997; Zehavi et al. 2002). From each SIMBAD query, we retain the R.A. (α), decl. (δ), m_g, m_B, and redshift of each MWA candidate. We assign the UDG candidate the redshift of the associated MWA, evaluate its absolute magnitude and size, reject candidates that do not match our physical size criteria for UDGs, and calculate the projected

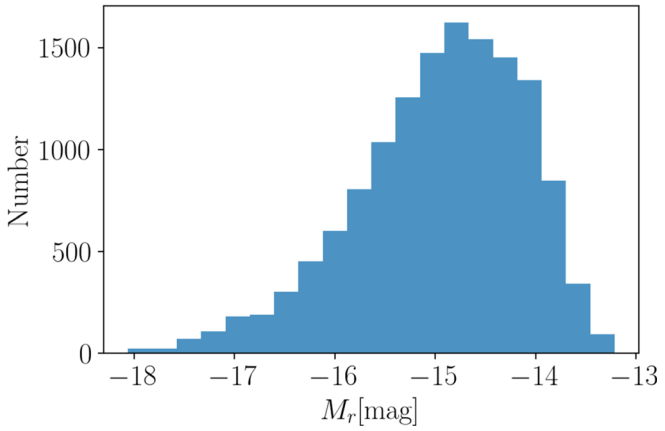

Figure 1. Distribution of inferred absolute magnitudes of UDG satellites when working within the $4500 < cz/(\mathrm{km\ s^{-1}}) < 5500$ slice. Although many of the galaxies are likely to be false pairs, this plot shows the type of UDG satellites to which we are sensitive.

physical separation between the pair. In Figure 1 we present the inferred absolute magnitude distribution of the candidate UDGs in the nearest slice. Although the majority of these values are drawn from unphysical pairs, and are therefore incorrect, the distribution does provide some guidance regarding the types of satellites to which this analysis is sensitive. These are satellites that are likely to be less luminous than the Small Magellanic Cloud but more luminous than the Fornax dSPh ($M_V = -16.8$ and -13.5, respectively; McConnachie 2012; with $V-r$ colors likely to be <1; Fukugita et al. 1995).

For completeness, we briefly describe the SMUDGes catalog here, but refer readers to the original papers for details of the search and verification procedures, and the uncertainty and completeness simulations. The candidate UDGs are selected to have half-light angular sizes larger than $5\farcs3$ and central g-band surface brightness of 24 mag arcsec^{-2} or fainter. SMUDGes begins significantly losing sensitivity at central surface brightness of 25.5 mag arcsec^{-2}, but does detect objects down to 26.9 mag arcsec^{-2} with 20% completeness. The angular size criterion was set to select galaxies with physical half-light radii larger than 2.5 kpc at the distance of the Coma cluster. We focus on the physically larger UDGs both on scientific grounds (the larger UDGs are the more massive and hence most interesting for a variety of reasons) and practical ones (the modeling is more robust for objects whose angular half-light radii are at least several times larger than the seeing). As described in previous papers (Zaritsky et al. 2019, 2021, 2022, 2023), we determine that our survey is highly complete in galaxies that match our selection and sensitivity criteria by comparing to existing catalogs (van Dokkum et al. 2015a; Román & Trujillo 2017a, 2017b; Leisman et al. 2017; Greco et al. 2018; Prole et al. 2018; Tanoglidis et al. 2021). Most of the published surveys include smaller galaxies than those in SMUDGes and some, e.g., Greco et al. (2018), detect galaxies with fainter central surface brightness, but SMUDGes has the largest areal coverage and is therefore well suited for the study of the rarer, larger UDGs. For detailed comparisons to previous work, we specifically point the reader to Section 4.2 of Zaritsky et al. (2022).

Our search produces a list of 626,560, 411,507, and 538,726 accepted UDG-MWA pairs for the three different redshift slices from the catalog of 6332 UDG candidates meeting our completeness criterion and the recovered 2905 MWAs across

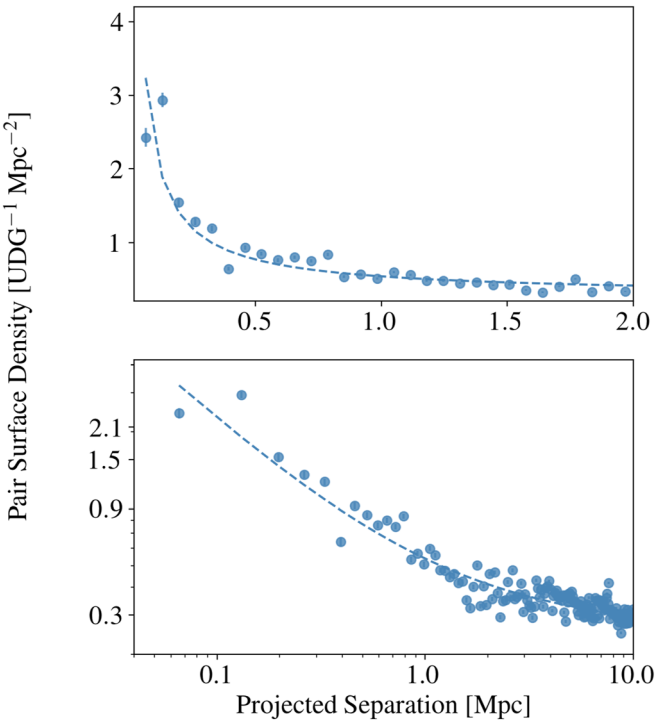

Figure 2. UDG-MWA pair surface density for the $4500 < cz/(\mathrm{km\ s^{-1}}) < 5500$ slice per UDG. The pairs are defined by their projected separation. The upper panel shows the distribution in linear units, while the lower one in logarithmic units. The power law + background model fit is performed in linear space but shown in both panels. Error bars are plotted, but are mostly within the symbols themselves. We discuss the apparent underestimation of the uncertainties in the text.

the three redshift slices. We track the distribution of pair separations, inversely weighted by the completeness fraction of each UDG separately for (1) all pairs, (2) those containing a blue UDG, and (3) those containing a red UDG. The color dividing line is defined to be 0.1 mag bluer than the empirically determined red sequence for UDGs ($g-r = 0.167 - 0.031M_r$; Zaritsky et al. 2022). We also set lower ($g-r > 0.2$) and upper ($g-r < 0.75$) color cutoffs to remove likely contaminants in the catalog (Zaritsky et al. 2022). The blue limiting criterion also matches the color of the bluest field UDGs examined in detail (Jones et al. 2023).

We present the pair separation distribution using 150 bins ($\sim$67 kpc wide) out to 10 Mpc for the nearest redshift slice (Figure 2). We estimate uncertainties using Poisson errors in the number of pairs in each bin and then propagate those through the calculation of the surface density. This is likely to be an underestimate of the uncertainties and we discuss the alternative approach below, but nevertheless use these estimates in our non-linear least square fitting. A simple power law plus constant background fit to the surface density, $\Sigma = ar^k + b$, is also shown in Figure 2 and appears to be a reasonable approximation to the data (numerical values for the fit parameters are given in Table 1 for each of the three redshift slices and color divided samples). The constant term represents the uncorrelated background and foreground that produce unphysical pairs. While the level of contamination will vary from MWA to MWA, on average (18% of the pairs with projected separations $\leqslant$250 kpc) it is modeled well out to large radii (Figure 2) and contributes little to the final uncertainty in our satellite counts as we describe further below.

Table 1
UDG-MWA Pair Separation Distribution Power-law Fit Parameters

UDG Sample	a	k	b
All, $4500 < cz/\mathrm{km\ s^{-1}} < 5500$	0.28 ± 0.02	-0.87 ± 0.07	0.26 ± 0.01
All, $5500 < cz/\mathrm{km\ s^{-1}} < 6500$	0.21 ± 0.01	-0.96 ± 0.05	0.18 ± 0.04
All, $6500 < cz/\mathrm{km\ s^{-1}} < 7500$	0.32 ± 0.01	-0.70 ± 0.04	0.21 ± 0.01
Red, $4500 < cz/\mathrm{km\ s^{-1}} < 5500$	0.39 ± 0.03	-0.86 ± 0.07	0.23 ± 0.01
Red, $5500 < cz/\mathrm{km\ s^{-1}} < 6500$	0.28 ± 0.02	-0.98 ± 0.05	0.17 ± 0.01
Red, $6500 < cz/\mathrm{km\ s^{-1}} < 7500$	0.38 ± 0.02	-0.73 ± 0.05	0.20 ± 0.01
Blue, $4500 < cz/\mathrm{km\ s^{-1}} < 5500$	0.07 ± 0.02	-1.23 ± 0.26	0.31 ± 0.01
Blue, $5500 < cz/\mathrm{km\ s^{-1}} < 6500$	0.10 ± 0.01	-0.96 ± 0.10	0.18 ± 0.04
Blue, $6500 < cz/\mathrm{km\ s^{-1}} < 7500$	0.25 ± 0.02	-0.56 ± 0.07	0.20 ± 0.01

There are, however, two potential problems with the model fits and their interpretation. First, as we mentioned above, we expect incompleteness to set in at small separations. The comparison of the data and the fitted power law in Figure 2 suggests a possible decline in pair surface density in the innermost bin, but with our current binning scheme there is no resolution at radii within $r < 100$ kpc. Whether the decline is observational, statistical, or physical is unclear.

To further examine the behavior of the pair separation distribution at radii within 100 kpc, we reduce the bin width to 20 kpc with the understood sacrifice of lower statistical precision. The comparison of the pair surface densities derived from the three redshift slices is presented in Figure 3. For this comparison, we scaled the three distributions to produce the same number density of background (uncorrelated) pairs. Although there is not an unambiguous systemic downturn among the distributions, a second potential problem becomes evident. The scatter among the measurements, even within one redshift slice, greatly exceeds the plotted statistical uncertainties, which are mostly smaller than the size of plotted symbols. We reevaluate the uncertainties using the scatter among the results from the three redshift slices and plot the mean and standard deviation of the mean the lower panel of Figure 3. This estimate of the uncertainties has the potential to be an overestimate as the surface density profiles among the slices may vary because the satellite samples in each slice are different in terms of luminosity and physical size. We expect the uncertainties to lie somewhere between those shown in Figures 2 and 3, but closer to the latter.

In the lower panel of Figure 3 we find a decline at the smallest radii (perhaps the innermost two or three bins), but the uncertainties are clearly larger than our previous estimates (excluding the innermost point, which is likely to have an actual uncertainty that is comparable to the other data within 100 kpc but just happened to contain measurements that exhibited little scatter). At the radii where this turnover might be detectable (~60 kpc) some of our largest galaxy masks may be affecting the completeness. Examining the sample of confirmed UDG satellites discussed by Karunakaran & Zaritsky (2023), we find no sign of such a turnover, but the numbers are small. On the other hand, if this turnover is real then it could signal an interesting physical effect. This topic is clearly an avenue that requires further study with larger samples. We will discuss the possible effect of this uncertainty in our measurements below. As for why the Poisson statistics underestimate the true uncertainties, we suspect that it is related to the fact that pairs are not statistically independent (for example, a single UDG will be paired with each of the L^* galaxies in a nearby galaxy group). Finally, the inclusion or exclusion of pairs with separations <60 kpc only modestly affects the fitting results. Comparing to the results presented in Table 1, most values change by $<1\sigma$ and none by more than 2σ when we exclude all pairs with projected separations <60 kpc in our fitting.

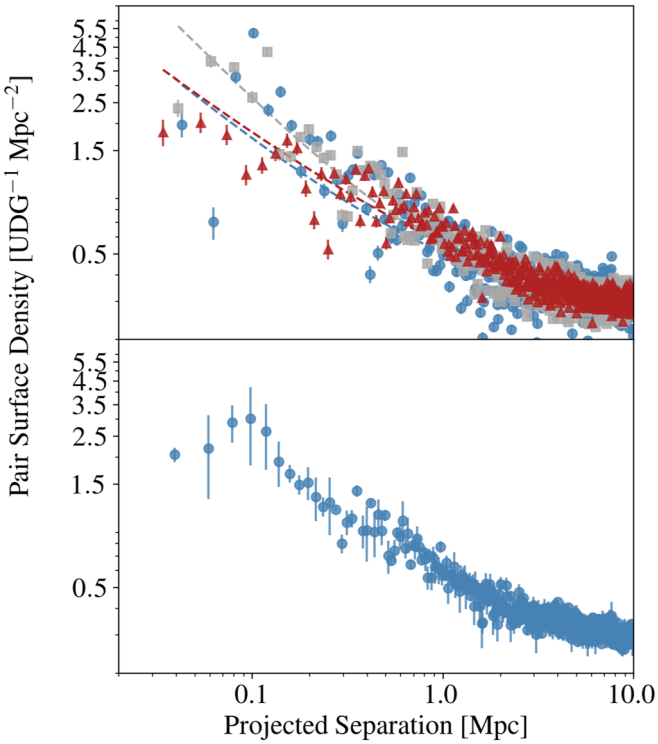

Figure 3. Comparison of pair separation distributions derived from the three redshift slices in the upper panel: $4500 < cz/\mathrm{km\ s^{-1}} < 5500$ (blue circles); $5500 < cz/\mathrm{km\ s^{-1}} < 6500$ (gray squares); $6500 < cz/\mathrm{km\ s^{-1}} < 7500$ (red triangles). We have decreased the bin size to 20 kpc and overplot the newly fitted model curves for each of the three redshift slices. In the lower panel we show the average of the three slices with the uncertainties reflecting the error in the mean using standard deviation of those values rather than the Poisson uncertainties shown in the upper panel.

To calculate the number of UDG satellites per MWA, S_{UDG}, we invert our measurements. The distribution of separations remains the same, but the normalization changes. The one aspect we do not know is the number of MWAs over the survey area (we only searched for MWAs projected near UDGs). We can however, estimate the surface density of MWAs in the

Table 2
Number of UDG Satellites per MWA

UDG Sample	$S_{\rm UDG}$
All, $4500 < cz/{\rm km\ s^{-1}} < 5500$	$0.53^{+0.10}_{-0.08}$
All, $5500 < cz/{\rm km\ s^{-1}} < 6500$	$0.46^{+0.05}_{-0.05}$
All, $6500 < cz/{\rm km\ s^{-1}} < 7500$	$0.25^{+0.02}_{-0.02}$
Red, $4500 < cz/{\rm km\ s^{-1}} < 5500$	$0.42^{+0.08}_{-0.07}$
Red, $5500 < cz/{\rm km\ s^{-1}} < 6500$	$0.36^{+0.05}_{-0.04}$
Red, $6500 < cz/{\rm km\ s^{-1}} < 7500$	$0.16^{+0.02}_{-0.02}$
Blue, $4500 < cz/{\rm km\ s^{-1}} < 5500$	$0.09^{+0.09}_{-0.04}$
Blue, $5500 < cz/{\rm km\ s^{-1}} < 6500$	$0.10^{+0.03}_{-0.02}$
Blue, $6500 < cz/{\rm km\ s^{-1}} < 7500$	$0.07^{+0.01}_{-0.01}$

survey footprint using the measured background values, b, of our model fits. By multiplying this surface density and the survey area, A, of the full survey (20,000 deg^2, converted to Mpc^2 using the mean distance of the relevant sample), we calculate the number of MWAs over the survey footprint ($\equiv A \cdot b$). Specifically, the number of UDGs associated with each MWA, for projected separations ranging from $r_{\rm min}$ to $r_{\rm max}$ is given by

$$S_{\rm UDG} = \frac{\int_{r_{\rm min}}^{r_{\rm max}} 2\pi a r^k r dr \cdot N_{\rm UDG}}{A \cdot b}, \quad (1)$$

where $N_{\rm UDG}$ is the number of UDG candidates in the sample being considered (as opposed to the number of UDG satellites, $S_{\rm UDG}$), and a, b, and k are the corresponding fit parameters for that sample.

We calculate $S_{\rm UDG}$ by integrating from 20 to 250 kpc. To estimate the uncertainties in $S_{\rm UDG}$, we evaluate the integral 1000 times, choosing different values for a, b, and k from their respective error distributions, and use the resulting distribution of $S_{\rm UDG}$ to define the 16th and 84th percentiles as the 1σ uncertainty interval. The inner boundary of our integration represents a radius at which we are effectively within the MWA itself but in practice eliminating this cut does not increase the inferred $S_{\rm UDG}$ beyond the quoted uncertainty. The outer boundary represents the extent of the MWA halo, or virial radius. While our MW may have a somewhat smaller virial radius (e.g., Shen et al. 2022), even decreasing the outer radius to 200 kpc reduces the inferred number of satellites only slightly below the quoted 1σ lower bound quoted in Table 2. Finally, to address the possibility of a turnover in $S_{\rm UDG}$ at small radii, if we integrate only from 70 kpc outward, where there is no hint of a turnover, $S_{\rm UDG}$ drops to 0.43 for the nearest redshift slice, which is a value that is only slightly more than a 1σ decrease from that quoted. We expect this to be an overestimate of the potential effect because we assumed in this test that there are absolutely no UDG satellites interior to 70 kpc even in projection. In fact, the region near the MWA may be a difficult one to interpret as there may be an additional contribution from UDG-like tidal dwarfs (Bennet et al. 2018).

Finally, we compare our choice to fit the physical pair distribution with a power law rather than a more physically motivated profile, such as a projected NFW profile (Navarro et al. 1996), as has been done for other satellite galaxy samples (Wang et al. 2014; van der Burg et al. 2016; Li et al. 2023b). To inform the discussion, we use COLOSSUS (Diemer 2018) to calculate a set of projected surface density profiles of MWA halos. The results turn out to be complex to interpret but informative.

We begin by exploring the resulting projected profile from an NFW halo tailored to match a MWA ($M_{200} = 1.08 \times 10^{12}\ M_\odot$; Shen et al. 2022; and $c = 10$). Such a halo produces a surface density profile from 60 to 250 kpc that is well matched by a radial power law of slope of -1.8. This slope value is as expected because NFW profiles at large radius tend to $\rho \propto r^{-3}$ and so in surface density to r^{-2}. However, this slope is significantly steeper than what we measure (~ -0.9; Table 1).

As emphasized by Diemer (2018), a halo does not exist in isolation but is surrounded both by infalling matter beyond $r_{\rm vir}$ and matter from correlated nearby structures. COLUSSUS offers a variety of approaches to model these additional complexities, including an option to use the matter correlation function to describe the additional contribution. Although this additional matter lies beyond $r_{\rm vir}$ in 3D, it contributes to the projected matter profile inside of $r_{\rm vir}$ because it is spatially correlated with the MWA. When we add this component to the model, using a bias parameter appropriate for a MWA halo, the resulting surface density distribution begins to show curvature, so the fitted power-law slope depends on the radial fitting range, but within reasonable choice of fitting radii we measure power-law slopes that are ~ -1.0. This result is both significantly different than the value obtained using the isolated NFW profile, demonstrating the sensitivity of the fitting to the treatment of matter beyond $r_{\rm vir}$, and it is much closer to what we measured. This exercise demonstrates that using a physically motivated profile introduces its own set of additional uncertainties.

The remaining puzzle is why our results are at odds with previous studies that concluded that an (isolated) NFW profile was a good fit to their measurements of the satellite distribution. Various factors may play a role. First, although Wang et al. (2014) find generally good agreement with an NFW model, they notice that the deviations are greatest for their most massive primaries, which are those that are most similar to our MWAs. The sense of the deviation is in line with our results. Second, Wang et al. (2012) select isolated primaries for their study. This is a typical approach when studying spectroscopically selected satellite populations to avoid confusion and it should minimize the contribution from matter beyond $r_{\rm vir}$. Such a selection should result in satellite surface density profiles that are more consistent with those of isolated halo models. Our sample has no isolation criteria. Third, the selection of the satellites themselves could affect the comparison. Li et al. (2023b) aim to study satellites that are mass-size outliers. As they describe, this selection results in a different sample than our use of the "standard" UDG criteria. If one hypothesizes that these outliers, for the sake of this discussion, are the result of a phenomenon that happens when a galaxy is near or within $r_{\rm vir}$ (such as, ram pressure stripping), then their sample may be composed only of satellites within $r_{\rm vir}$, with little or no contribution from satellites in the infall region or in the broader local environment. If so, then an isolated NFW profile would be the better match. As such, finding a match to an isolated NFW model may have interesting implications for those satellite galaxies. Finally, van der Burg et al. (2016) examined UDG satellites in more massive halos ($\langle M_{200} \rangle = 5 \times 10^{14}\ M_\odot$). For such systems, the resulting isolated halo slope is somewhat shallower (slope $= -1.6$) and the effect of adding the correlated matter is more modest (resulting in slope $= -1.2$), but again the effect of the matter beyond $r_{\rm vir}$ is to make the slope shallower

than that of an isolated NFW halo. Indeed van der Burg et al. (2016) concluded that an (isolated) NFW halo profile did not fit their data.

3. Results

3.1. The UDG-MWA Pair Separation Distribution

In Figures 2 and 3, and in Table 1, we present our measurements of the UDG-MWA pair separation distribution. The rise in the surface density toward smaller separations demonstrates that there does exist a significant population of UDGs that are physically correlated with MWAs. Additionally, the mean power-law-slope fit for three slices (-0.84 ± 0.06) is in agreement with that for "normal" satellites of giant galaxies (~ -0.9; Lorrimer et al. 1994). UDGs do not appear to preferentially form or get destroyed in the environments near MWAs at different relative rates than do "normal" satellites. This conclusion comes with the caveat that we have insufficient data to explore trends at radii smaller than about 60 kpc. Environment, at least broadly within the virial radius of MWAs, does not appear to be a significant factor in the evolution of the number of UDGs. This result is in concordance with a lack of any strong environmental signature in the approximately linear relation between the number of UDGs per halo and host halo mass extending from the most massive galaxy clusters down to MWAs (Karunakaran & Zaritsky 2023; Li et al. 2023b), which we will further confirm in Section 3.2.

Regarding UDG-formation mechanisms, these results indicate that UDGs—at least the population of satellite UDGs—form primarily as part of the normal, hierarchical universal dark-matter superstructure (e.g., Di Cintio et al. 2017; Chan et al. 2018; Jiang et al. 2019; Martin et al. 2021; Wright et al. 2021), rather than through more specific channels like UDG formation through tidal interactions (Bennet et al. 2018; Jones et al. 2021), direct satellite collisions (Silk 2019; Shin et al. 2020), or interaction with extremely dense environments (Yozin & Bekki 2015; Safarzadeh & Scannapieco 2017) that may best explain interesting individual UDGs. Of course, even within the "standard" model, formation for such a heterogeneous class of objects as UDGs may follow several formation pathways (Liao et al. 2019; Sales et al. 2020), and our measurement is insensitive to UDG satellites found at small separations.

3.2. The Number of Satellite UDGs per MWA

Using the pair separation density profiles, we calculate and present the number of UDG satellites for the typical MWA within projected radii between 20 and 250 kpc in Table 2. Aside from the statistical errors that are quoted, these numbers are susceptible to various systematic uncertainties. First, the sample of UDGs is incomplete, as we will discuss in Section 3.4. Second, as we have discussed already, the appropriate limits on the integration of the radial surface density profile are somewhat uncertain, which results in uncertainties that are comparable to the statistical ones. Lastly, we are working with projected rather than physical radii.

Focusing for now only on the full samples (not selecting by color), and using only the lower redshift slice—where we do not suffer additional incompleteness related to size—we find that, within the range of UDG properties that we are sensitive to, the typical MWA contains less than one UDG satellite

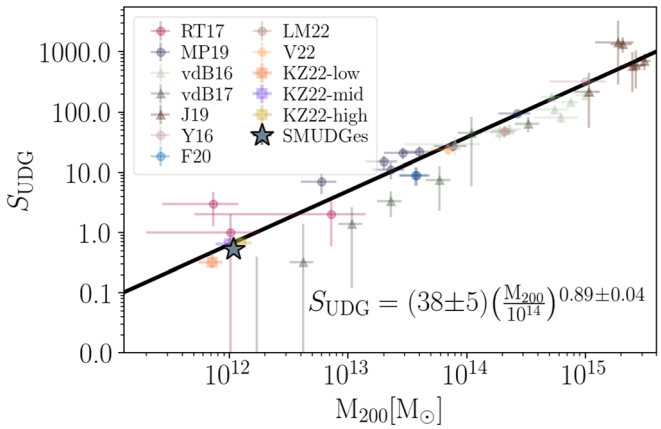

Figure 4. $S_{\rm UDG}$, derived from the nearest redshift slice, vs. host halo mass. We adopt the MW mass estimate of Shen et al. (2022) to represent our MWAs. The plot, the fitted relationship, and other measurements are adopted directly from Karunakaran & Zaritsky (2023), and the original measurements referenced in the legend (Román & Trujillo 2017b; Mancera Piña et al. 2019; van der Burg et al. 2016, 2017; Janssens et al. 2019; Yagi et al. 2016; Forbes et al. 2020; La Marca et al. 2022a; Venhola et al. 2022).

(0.5 ± 0.1). This result does not change if we exclude pairs with projected separations <60 kpc.

We place this result in context in Figure 4, reprised from Karunakaran & Zaritsky (2023), by comparing the number of UDG satellites per MWA, $S_{\rm UDG}$, to the numbers of UDG satellites measured in host halos of similar or larger masses. The comparison is somewhat fraught because the data come from a variety of surveys that have different selection criteria. Such differences tend to be of order unity and are obscured by the large parameter range covered in the figure, but they need to be carefully addressed if one is interested in modest deviations from a linear slope in the overall relation. Nevertheless, we confirm the qualitative conclusion of previous studies (Li et al. 2023b; Karunakaran & Zaritsky 2023) that $S_{\rm UDG}$ for MWAs is approximately consistent with a linear extrapolation of the relation established using halos of larger total mass.

At a quantitative level such comparisons are complicated by different data quality and selection criteria across the studies. For example Li et al. (2023b) reach significantly fainter surface brightness levels and define their sample on the basis of mass rather than just the directly observed quantities usually used to define UDGs. Proceeding to make the comparison even so, they find 0.44 ± 0.05 UDGs per MWA, compared to our value of 0.5 ± 0.1. Independently, the Karunakaran & Zaritsky (2023) relationship suggests each MWA has 0.6 UDG satellites. Given likely systematic differences among samples, the range of values provides guidance regarding uncertainties involved in this measurement.

The near linearity of this relation over more than 3 orders of magnitude in mass might appear to challenge models where UDG satellites are a hybrid population; for example, those where a significant fraction of UDG satellites are born as such and the remainder consists of galaxies transformed by the environment (Liao et al. 2019; Sales et al. 2020). However, at least in terms of the number of UDG satellites, the Liao et al. (2019) study is consistent with our finding—predicting ~1 UDG satellite per MWA from their simulations, as well as the extrapolation of earlier work by Rong et al. (2017). Nevertheless, there is likely to be a fine-tuning challenge if simulations showing that only a small fraction of UDGs that

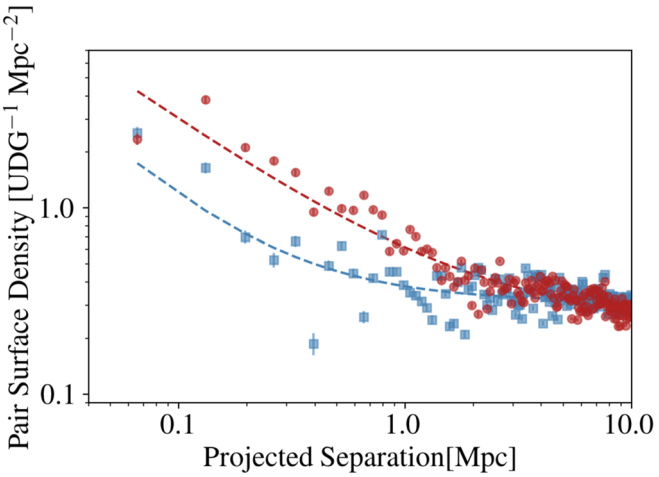

Figure 5. Pair surface density as a function of UDG color for the lowest redshift sample. UDG-MWA pairs that include a UDG classified as red are shown in the red circles, while those classified as blue are shown as blue squares. Dashed lines are power law plus flat background fits to the data.

fall into clusters survive (∼20%; Jiang et al. 2019) are correct. This challenge could become acute when a precise slope is empirically determined. A version of Figure 4 redone with homogeneous data and selection is critical to further confrontation to the models.

3.3. UDG Satellite Colors

We now examine the behavior of red and blue UDGs separately. In Figure 5 we present the pair separation distribution for red and blue UDGs in the redshift slice spanning $4500 < cz/(\mathrm{km\ s^{-1}}) < 5500$. The results for the other slices are similar. While the surface density rise at small separations is present in both populations, confirming the existence of both red and blue UDG satellite populations, it is dominated by red UDGs, indicating that the majority of UDG satellites of MWAs have not recently been forming stars at a significant rate. Roughly 80% of the UDG satellites we find are red. Despite differences in samples that we have already discussed, this result is in excellent agreement with the UDG quenched fraction measured by Li et al. (2023a).

In contrast to our conclusion regarding the number of UDGs, there is a strong environmental signature in the stellar populations of UDG satellites. Interestingly, however, there are some star-forming UDGs even at small (projected) separations, suggesting that whatever environmental quenching there may be is either not rapid or entirely efficient. This result follows on the suggestion from Karunakaran et al. (2021) that the overall satellite populations of galaxies indicate that quenching may be overestimated in current simulations. We close by noting that the divergence by color in the populations is evident even at large radii (>1 Mpc), well outside the virial radii of MWAs, much like it is in the general galaxy population surrounding galaxy clusters (Lewis et al. 2002; Gómez et al. 2003). As such, it suggests that much like for more massive galaxies, a full understanding of the environmental effects will be challenging to reach and must involve preprocessing (Zabludoff & Mulchaey 1998; McGee et al. 2009; De Lucia et al. 2012) that occurs prior to the galaxy's arrival in its current environment.

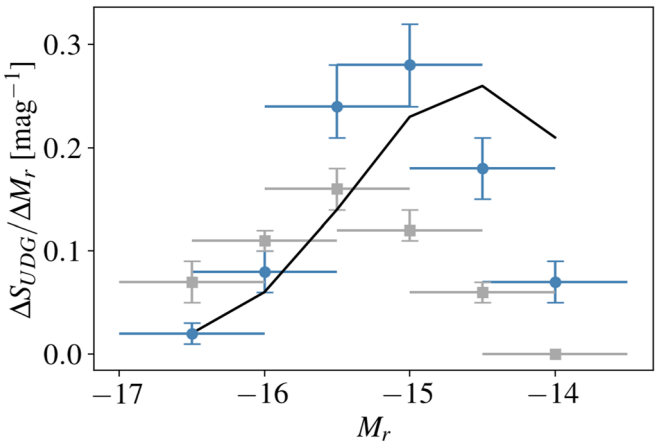

Figure 6. UDG satellite luminosity function. We present the number of UDG satellites within 1 magnitude bins as derived from our three redshift slices. The results for the nearest slice ($4500 < cz/(\mathrm{km\ s^{-1}}) < 5500$) are represented by the black line, while those of the other two slices are represented by blue circles and gray squares, with the squares representing the farthest of the three slices. Horizontal bars represent the bin widths, while vertical error bars are statistical uncertainties. Units for ΔS_{UDG}, are number per MWA per magnitude.

Table 3
Number of UDG Satellites per MWA in Luminosity Bins

Luminosity Range	$4500 < cz/\mathrm{km\ s^{-1}} < 5500$	$5500 < cz/\mathrm{km\ s^{-1}} < 6500$	$6500 < cz/\mathrm{km\ s^{-1}} < 7500$
$-17.0 < M_r < -16.0$	$0.02^{+0.16}_{-0.03}$	$0.02^{+0.01}_{-0.01}$	$0.07^{+0.02}_{-0.02}$
$-16.5 < M_r < -15.5$	$0.06^{+0.06}_{-0.03}$	$0.08^{+0.02}_{-0.02}$	$0.11^{+0.01}_{-0.01}$
$-16.0 < M_r < -15.0$	$0.14^{+0.03}_{-0.03}$	$0.24^{+0.04}_{-0.03}$	$0.16^{+0.02}_{-0.02}$
$-15.5 < M_r < -14.5$	$0.23^{+0.05}_{-0.04}$	$0.28^{+0.04}_{-0.04}$	$0.12^{+0.02}_{-0.01}$
$-15.0 < M_r < -14.0$	$0.26^{+0.06}_{-0.05}$	$0.18^{+0.03}_{-0.03}$	$0.06^{+0.01}_{-0.01}$
$-14.5 < M_r < -13.5$	$0.21^{+0.07}_{-0.05}$	$0.07^{+0.02}_{-0.02}$	$0.00^{+0.00}_{-0.00}$

3.4. UDG Satellite Luminosity Function

For each of the three redshift slices, we present the number of UDG satellites per magnitude over the range of magnitudes to which we are sensitive in Table 3 and Figure 6. These values are evaluating by reprising the analysis for S_{UDG} using only pairs where the putative satellites fall in the magnitude bin for each of the magnitude bins. Together these provide both a selection-uncorrected view of the UDG satellite luminosity function and the associated uncertainties.

The results among the three redshift slices agree well down to $M_r \sim -15$ and then begin to diverge. That divergence is systematic in that the decline in numbers with fainter luminosity begins at brighter luminosity with the most distant redshift slice and continues in sequence up until the nearest slice. This behavior is as expected because we are less sensitive both to fainter and smaller UDG satellites at larger distances. Even in the intermediate redshift slice, the SMUDGes angular selection criterion already excludes UDGs with physical effective radii of less than about 2 kpc. For reference, our 5.3 arscec cut in r_e corresponds to 1.8, 2.2, and 2.5 kpc at the midpoint distance of each of the three slices. The turnover in the luminosity function obtained from the nearest redshift slice suggests that it too is incomplete below $M_r \sim -15$. If so, then this means that the total satellite numbers we provide in Section 3.2 are, to some degree, underestimates of the full number of UDG satellites. However, there are reasons to believe that the UDG population does not extend in large

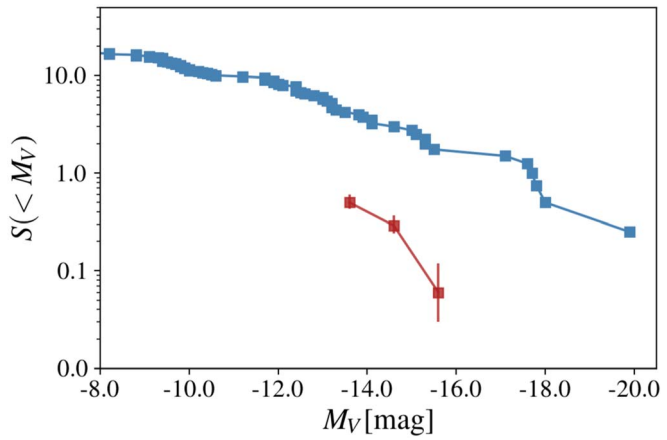

Figure 7. Comparison of the average cumulative satellite luminosity function for local MWAs (data from Bennet et al. 2019 and references thererin; see text) in blue and our measurements for UDG satellites of MWAs in the nearest redshift slice in red. At a given luminosity, over the range of our measurements, UDG satellites are typically about ∼10% of the total number of satellites.

numbers to fainter surface brightnesses than those captured by SMUDGes (Zaritsky et al. 2022).

To place these numbers in context, we compare our luminosity function for UDG satellites with the satellite luminosity functions of four nearby, extremely well-studied MWAs (M 84, M 91, M 101, and Cen A; Bennet et al. 2019, and references therein) in Figure 7. We show the cumulative satellite luminosity function for the combined set of nearby MWAs and that for our UDG satellites in our nearest redshift slice. We have corrected our values of M_r to M_V using a mean value of $g-r$ of 0.6 for UDGs and a correction (Fukugita et al. 1995) from V to g of 0.2 mag for early type galaxies (80% of UDG satellites are non-star-forming; Section 3.3). We expect that the published luminosity functions for the local MWAs include any UDG satellites that are there because those studies used deep, wide field observations intended to reach both faint and low luminosity systems. For $-16 < M_V < -14$, we find that UDG satellites are ∼10% of the satellite population. We conclude that the UDG satellite population at a given luminosity, for $M_V < -14$, is subdominant, and there is no significant lurking population of large low-surface-brightness satellites at these luminosities.

3.5. UDG Satellite Mass Function

A mass function measurement would be ideal for a direct comparison to models. Although cosmological simulations do produce UDGs (Tremmel et al. 2020; Wright et al. 2021), we are always at the mercy of assumptions in the baryonic subgrid physics if we can only compare the luminous properties of galaxies. A check on those assumptions would be to have both the luminosities and masses of UDGs (or at least internal kinematics). As we mentioned previously, the total mass-to-light ratios, $(M/L)_{\rm total}$, of UDGs are likely to be significantly larger than those of comparably massive galaxies. At the limit of our current understanding of UDGs, they appear to have $(M/L)_{\rm total}$ that is at least an order of magnitude larger (van Dokkum et al. 2019), with perhaps some unusual exceptions (van Dokkum et al. 2022). If indeed $(M/L)_{\rm total}$ for UDG satellites is a factor of 10 larger than for non-UDG satellites of similar luminosity, then we should slide the UDG LF in Figure 7 to the right by 2.5 magnitudes to appropriately compare the numbers of similarly *massive* satellites. At this point, the UDG satellites would still be subdominant in number, but now only by a factor of a few rather than an order of magnitude. As such, they could play a significant role in the satellite/subhalo accounting at LMC-like masses.

To explore this topic a bit further, we estimate the total mass of these low-mass galaxies using only photometry (Zaritsky & Behroozi 2023). In this approach, a scaling relation is used to recover the velocity dispersion at the effective radius, and therefore an estimate of the enclosed mass within this radius. By assuming an NFW density profile (Navarro et al. 1996), we then determine which model produces the measured enclosed mass at r_e. The method was used by Zaritsky & Behroozi (2023) to explore the stellar mass-halo mass relation and by Zaritsky (2022) to study the relation between globular cluster populations and total mass. We use the relation to isolate UDGs with masses comparable to or larger than that of the LMC ($\log(M_h/M_\odot) = 11.14$; Erkal et al. 2019). We present results for pair separation involving UDGs inferred to have $10.9 < \log(M_h/M_\odot) < 12$. As a caution, we note that the scaling relation has not been fully vetted to apply to UDGs because of the paucity of spectroscopic data for UDGs. Where comparison is possible, the results are in acceptable agreement and provide masses within a factor of a few, which is comparable to the overall precision limit of the method and within the range of our order of magnitude mass selection bin. Further discussion of the use of this approach is presented in Zaritsky et al. (2023).

We find results from the three slices that are consistent for the number of LMC-mass or greater, UDG satellites per MWA ($0.08^{+0.08}_{-0.04}$, $0.06^{+0.04}_{-0.03}$, and 0.07 ± 0.1, for the lowest to highest redshift slices, respectively). The numbers across the slices are similar because the mass requirement results in all of these UDGs having $r_e > 3$ kpc and, therefore, there is no relative size bias across the three slices. Averaging, we obtain that the number of UDG satellites with LMC-like or larger masses per MWA is $0.07^{+0.04}_{-0.04}$, or alternatively corresponding to ∼13% of our deepest satellite sample (the lowest redshift sample). Roughly 1 in 14 MWAs have a UDG satellite that is of comparable mass to the LMC. Comparing that result to the calculation based on standard ΛCDM that ∼40% of 10^{12} M_{200} halos should host something nearly as massive as the LMC (Wang et al. 2012) suggests that ∼18% of this population may fall in the ultradiffuse class.

4. Conclusions

We present a correlation analysis between UDG candidates from the SMUDGes catalog (Zaritsky et al. 2019, 2022, 2023) and Milky Way analogs (MWAs) drawn from the SIMBAD database (Wenger et al. 2000) from which we identify a population of UDGs that are physically associated with MWAs. We find the following:

1. A population of UDG satellites exists that surrounds MWAs. The distribution of those satellites (projected surface density $\propto r^{-0.84\pm0.06}$) is entirely consistent in character with that of normal satellite galaxies. We conclude that the processes by which most of these UDG satellites form are related to how low-mass galaxies form in general. We exclude exotic formation mechanisms for UDG satellites as a primary formation channel. A consistent conclusion was reached in a recent study of

an entirely different population of UDGs (Jones et al. 2023).

2. On average, each MWA has $\sim 0.5 \pm 0.1$ UDG satellites at projected radii between 20 and 250 kpc and $-17 < M_r < -13.5$. This value is calculated using only the nearest of our three redshift samples to ensure that we are as close as possible to being complete down to $r_e = 1.5$ kpc.
3. We compare our measurement of the number of UDG satellites per MWA to published measurements of the number of UDG satellites in hosts of different masses. We confirm previous findings that the number of UDG satellites of MWAs is consistent with a nearly linear trend between the number of UDG satellites and total halo mass (Li et al. 2023b; Karunakaran & Zaritsky 2023). We interpret this finding as providing further evidence against specific, UDG-formation scenarios that are unconnected with the general formation path of low-mass galaxies.
4. We find that red UDGs are far more tightly clustered around MWAs than blue UDGs and that red UDGs comprise $\sim$80% of the UDG satellite population of MWAs out to 250 kpc (where blue is defined as being more than 0.1 mag bluer than the red sequence in $g - r$ versus M_r). Although environmental quenching is likely involved, we note that—as with normal galaxies near galaxy clusters (Lewis et al. 2002; Gómez et al. 2003)—the color changes happen well outside the virial radius, and the trend likely results from a far more complex history (e.g., De Lucia et al. 2012) than that proposed in simple quenching scenarios.
5. We find that for $-17 < M_r < -13.5$ UDG satellites are $\sim$10% of the total satellite population down to a similar magnitude limit. However, we note that UDGs have been shown in the limited number of cases studied to be strongly dark-matter dominated, and may therefore represent a larger fraction of satellites down to a correspondingly larger total mass limit. In support of this claim we estimate halo masses using the Zaritsky & Behroozi (2023) methodology and conclude that UDG satellites may comprise $\sim$18% of the satellites with halo masses of at least half the mass of the LMC.

In summary, UDG satellites appear to be directly connected to the overall satellite population in a manner that suggests that there is not a distinct, separate formation channel. They are a minority, but still significant fraction of the satellite populations of Milky Way analogs and should be included in discussions involving satellite galaxy populations.

Acknowledgments

The authors thank the referee for insightful comments that improved the clarity of the manuscript and led to the discussion comparing the power-law empirical profile to a physically motivated NFW one. The authors acknowledge financial support from NSF AST-1713841 and AST-2006785 for SMUDGes. An allocation of computer time from the UA Research Computing High Performance Computing (HPC) at the University of Arizona and the prompt assistance of the associated computer support group is also gratefully acknowledged. A.K. acknowledges financial support from the grant CEX2021-001131-S funded by MCIN/AEI/ 10.13039/ 501100011033 and from the grant POSTDOC_21_00845 funded by the Economic Transformation, Industry, Knowledge and Universities Council of the Regional Government of Andalusia.

Software: Astropy (Astropy Collaboration et al. 2013, 2018), astroquery (Ginsburg et al. 2019), galpy, (Bovy 2015), Matplotlib (Hunter 2007), NumPy (van der Walt et al. 2011), pandas (McKinney 2010), SciPy (Oliphant 2007; Millman & Aivazis 2011).

ORCID iDs

Hina Goto https://orcid.org/0000-0002-0268-5707
Dennis Zaritsky https://orcid.org/0000-0002-5177-727X
Ananthan Karunakaran https://orcid.org/0000-0001-8855-3635
Richard Donnerstein https://orcid.org/0000-0001-7618-8212
David J. Sand https://orcid.org/0000-0003-4102-380X

References

Astropy Collaboration, Price-Whelan, A. M., Sipőcz, B. M., et al. 2018, AJ, 156, 123
Astropy Collaboration, Robitaille, T. P., Tollerud, E. J., et al. 2013, A&A, 558, A33
Bennet, P., Sand, D. J., Crnojević, D., et al. 2019, ApJ, 885, 153
Bennet, P., Sand, D. J., Zaritsky, D., et al. 2018, ApJL, 866, L11
Bland-Hawthorn, J., & Gerhard, O. 2016, ARA&A, 54, 529
Blanton, M. R., Lupton, R. H., Schlegel, D. J., et al. 2005, ApJ, 631, 208
Bovy, J. 2015, ApJS, 216, 29
Carlsten, S. G., Greene, J. E., Greco, J. P., Beaton, R. L., & Kado-Fong, E. 2021, ApJ, 922, 267
Chan, T. K., Kereš, D., Wetzel, A., et al. 2018, MNRAS, 478, 906
Chilingarian, I. V., Afanasiev, A. V., Grishin, K. A., Fabricant, D., & Moran, S. 2019, ApJ, 884, 79
Crnojević, D., Sand, D. J., Spekkens, K., et al. 2016, ApJ, 823, 19
De Lucia, G., Weinmann, S., Poggianti, B. M., Aragón-Salamanca, A., & Zaritsky, D. 2012, MNRAS, 423, 1277
Di Cintio, A., Brook, C. B., Dutton, A. A., et al. 2017, MNRAS, 466, L1
Diemer, B. 2018, ApJS, 239, 35
Erkal, D., Belokurov, V., Laporte, C. F. P., et al. 2019, MNRAS, 487, 2685
Ferrarese, L., Côté, P., MacArthur, L. A., et al. 2020, ApJ, 890, 128
Forbes, D. A., Dullo, B. T., Gannon, J., et al. 2020, MNRAS, 494, 5293
Fukugita, M., Shimasaku, K., & Ichikawa, T. 1995, PASP, 107, 945
Geha, M., Wechsler, R. H., Mao, Y.-Y., et al. 2017, ApJ, 847, 4
Ginsburg, A., Sipőcz, B. M., Brasseur, C. E., et al. 2019, AJ, 157, 98
Gómez, P. L., Nichol, R. C., Miller, C. J., et al. 2003, ApJ, 584, 210
Greco, J. P., Greene, J. E., Strauss, M. A., et al. 2018, ApJ, 857, 104
Greene, J. E., Greco, J. P., Goulding, A. D., et al. 2022, ApJ, 933, 150
Guo, Q., Cole, S., Eke, V., & Frenk, C. 2012, MNRAS, 427, 428
Hinshaw, G., Larson, D., Komatsu, E., et al. 2013, ApJS, 208, 19
Holmberg, E. 1969, ArA, 5, 305
Hunter, J. D. 2007, CSE, 9, 90
Janssens, S. R., Abraham, R., Brodie, J., Forbes, D. A., & Romanowsky, A. J. 2019, ApJ, 887, 92
Jiang, F., Dekel, A., Freundlich, J., et al. 2019, MNRAS, 487, 5272
Jones, M. G., Bennet, P., Mutlu-Pakdil, B., et al. 2021, ApJ, 919, 72
Jones, M. G., Karunakaran, A., Bennet, P., et al. 2023, ApJL, 942, L5
Kadowaki, J., Zaritsky, D., Donnerstein, R., et al. 2021, ApJ, 923, 257
Karunakaran, A., Spekkens, K., Oman, K. A., et al. 2021, ApJL, 916, L19
Karunakaran, A., & Zaritsky, D. 2023, MNRAS, 519, 884
La Marca, A., Iodice, E., Cantiello, M., et al. 2022a, A&A, 665, A105
La Marca, A., Peletier, R., Iodice, E., et al. 2022b, A&A, 659, A92
Leisman, L., Haynes, M. P., Janowiecki, S., et al. 2017, ApJ, 842, 133
Lewis, I., Balogh, M., De Propris, R., et al. 2002, MNRAS, 334, 673
Li, J., Greene, J. E., Greco, J., et al. 2023a, ApJ, 955, 2
Li, J., Greene, J. E., Greco, J. P., et al. 2023b, ApJ, 955, 1
Liao, S., Gao, L., Frenk, C. S., et al. 2019, MNRAS, 490, 5182
Lorrimer, S. J., Frenk, C. S., Smith, R. M., White, S. D. M., & Zaritsky, D. 1994, MNRAS, 269, 696
Mancera Piña, P. E., Aguerri, J. A. L., Peletier, R. F., et al. 2019, MNRAS, 485, 1036
Mao, Y.-Y., Geha, M., Wechsler, R. H., et al. 2021, ApJ, 907, 85

Martin, G., Jackson, R. A., Kaviraj, S., et al. 2021, MNRAS, 500, 4937
McConnachie, A. W. 2012, AJ, 144, 4
McGee, S. L., Balogh, M. L., Bower, R. G., Font, A. S., & McCarthy, I. G. 2009, MNRAS, 400, 937
McKinney, W. 2010, in Proc. of the 9th Python in Science Conf. (Austin, TX: SciPy)
Millman, K. J., & Aivazis, M. 2011, CSE, 13, 9
Nashimoto, M., Tanaka, M., Chiba, M., et al. 2022, ApJ, 936, 38
Navarro, J. F., Frenk, C. S., & White, S. D. M. 1996, ApJ, 462, 563
Oke, J. B. 1964, ApJ, 140, 689
Oke, J. B., & Gunn, J. E. 1983, ApJ, 266, 713
Oliphant, T. E. 2007, CSE, 9, 10
Park, H. S., Moon, D.-S., Zaritsky, D., et al. 2017, ApJ, 848, 19
Prada, F., Vitvitska, M., Klypin, A., et al. 2003, ApJ, 598, 260
Prole, D. J., Davies, J. I., Keenan, O. C., & Davies, L. J. M. 2018, MNRAS, 478, 667
Román, J., & Trujillo, I. 2017a, MNRAS, 468, 703
Román, J., & Trujillo, I. 2017b, MNRAS, 468, 4039
Rong, Y., Guo, Q., Gao, L., et al. 2017, MNRAS, 470, 4231
Safarzadeh, M., & Scannapieco, E. 2017, ApJ, 850, 99
Sales, L., & Lambas, D. G. 2005, MNRAS, 356, 1045
Sales, L. V., Navarro, J. F., Peñafiel, L., et al. 2020, MNRAS, 494, 1848
Sales, L. V., Wang, W., White, S. D. M., & Navarro, J. F. 2013, MNRAS, 428, 573
Samuel, J., Wetzel, A., Santistevan, I., et al. 2022, MNRAS, 514, 5276
Shen, J., Eadie, G. M., Murray, N., et al. 2022, ApJ, 925, 1
Shin, E.-j., Jung, M., Kwon, G., et al. 2020, ApJ, 899, 25
Silk, J. 2019, MNRAS, 488, L24
Tanoglidis, D., Drlica-Wagner, A., Wei, K., et al. 2021, ApJS, 252, 18
Tremmel, M., Wright, A. C., Brooks, A. M., et al. 2020, MNRAS, 497, 2786
Tucker, D. L., Oemler, A. J., Kirshner, R. P., et al. 1997, MNRAS, 285, L5
van der Burg, R. F. J., Hoekstra, H., Muzzin, A., et al. 2017, A&A, 607, A79
van der Burg, R. F. J., Muzzin, A., & Hoekstra, H. 2016, A&A, 590, A20
van der Walt, S., Colbert, S. C., & Varoquaux, G. 2011, CSE, 13, 22
van Dokkum, P., Shen, Z., Keim, M. A., et al. 2022, Natur, 605, 435
van Dokkum, P., Wasserman, A., Danieli, S., et al. 2019, ApJ, 880, 91
van Dokkum, P. G., Abraham, R., Merritt, A., et al. 2015a, ApJL, 798, L45
van Dokkum, P. G., Romanowsky, A. J., Abraham, R., et al. 2015b, ApJL, 804, L26
Venhola, A., Peletier, R., Laurikainen, E., et al. 2017, A&A, 608, A142
Venhola, A., Peletier, R. F., Salo, H., et al. 2022, A&A, 662, A43
Wang, J., Frenk, C. S., Navarro, J. F., Gao, L., & Sawala, T. 2012, MNRAS, 424, 2715
Wang, W., Sales, L. V., Henriques, B. M. B., & White, S. D. M. 2014, MNRAS, 442, 1363
Wang, W., & White, S. D. M. 2012, MNRAS, 424, 2574
Weinberg, D. H., Bullock, J. S., Governato, F., Kuzio de Naray, R., & Peter, A. H. G. 2015, PNAS, 112, 12249
Wenger, M., Ochsenbein, F., Egret, D., et al. 2000, A&AS, 143, 9
Wright, A. C., Tremmel, M., Brooks, A. M., et al. 2021, MNRAS, 502, 5370
Yagi, M., Koda, J., Komiyama, Y., & Yamanoi, H. 2016, ApJS, 225, 11
Yozin, C., & Bekki, K. 2015, MNRAS, 452, 937
Zabludoff, A. I., & Mulchaey, J. S. 1998, ApJ, 496, 39
Zaritsky, D. 2022, MNRAS, 513, 2609
Zaritsky, D., & Behroozi, P. 2023, MNRAS, 519, 871
Zaritsky, D., Donnerstein, R., Dey, A., et al. 2019, ApJS, 240, 1
Zaritsky, D., Donnerstein, R., Dey, A., et al. 2023, ApJS, 267, 27
Zaritsky, D., Donnerstein, R., Karunakaran, A., et al. 2021, ApJS, 257, 60
Zaritsky, D., Donnerstein, R., Karunakaran, A., et al. 2022, ApJS, 261, 11
Zaritsky, D., Smith, R., Frenk, C., & White, S. D. M. 1993, ApJ, 405, 464
Zehavi, I., Blanton, M. R., Frieman, J. A., et al. 2002, ApJ, 571, 172